

High resolution spectroscopy of the “ ΣN cusp”
by using the $d(K^-, \pi^-)$ reaction

Co-spokespersons: Y. Ichikawa and K. Tanida

M. Fujita, S. Hasegawa, T. Hashimoto, Y. Ichikawa,
H. Sako, S. Sato, K. Tanida, T.O. Yamamoto
Japan Atomic Energy Agency (JAEA), Japan

S.H. Hayakawa, K. Miwa, H. Tamura
Tohoku University, Japan

T. Gogami, T. Harada, T. Nagae, T. Nanamura
Kyoto University, Japan

S. Ishimoto, S. Suzuki, M. Ukai
High Energy Accelerator Research Organization (KEK), Japan

J.K. Ahn, S.W. Choi, W.S. Jung, B.M. Kang, S.H. Kim, S.B. Yang
Korea University, Korea

December 20, 2021

Short summary of the Proposed Experiment

Beamline:	K1.8
Beam:	1.4 GeV/c K^-
Beam intensity:	5×10^5 /spill
Flat-top:	2 sec (4 sec/spill)
Target:	Liquid deuterium ϕ 54 mm
Reaction:	$d(K^-, \pi^-)$
Spectrometer etc.:	S-2S + HypTPC
Beam time:	15 days (Physics run) + 5 days (Empty run) + 1 day H_2 target run + 3 days for detector commissioning
Estimated Yield:	1.4×10^4 events

Abstract

We propose to measure the missing-mass spectrum around the ΣN threshold in the $d(K^-, \pi^-)$ reaction at 1.4 GeV/c. A clear enhancement was observed near the ΣN threshold, so called “ ΣN cusp”, for a long time ago. However, the dynamical origin of this enhancement remains unclear as yet. Especially, whether “ ΣN cusp” is cusp or unstable bound state has not been determined yet. One of the key to make it clear is to improve the missing-mass resolution and statistics. We can achieve the missing-mass resolution of 0.4 MeV in σ by using K1.8 beam line and S-2S spectrometers at J-PARC. We will install HypTPC to suppress quasi-free backgrounds by detecting the charged tracks of the decay products. We can deduce the scattering length of ΣN system with isospin $T = 1/2$ and spin triplet channel in this experiment.

1 Physics motivation

An enhancement near the ΣN threshold (~ 2.13 GeV/ c^2) was clearly observed in the $K^- d \rightarrow \pi^- \Lambda p$ reaction at rest more than 50 years ago [1]. This enhancement is called as “ ΣN cusp”, while whether “ ΣN cusp” is cusp (inelastic virtual state) or unstable bound state has not been confirmed yet. The “ ΣN cusp” was measured by various experiments using $K^- d \rightarrow \pi^- \Lambda p$, $\pi^+ d \rightarrow K^+ \Lambda p$, and $pp \rightarrow K^+ \Lambda p$ reactions [2, 3, 4, 5, 6, 7, 8]. Recently, the “ ΣN cusp” has also been observed by the Λ - p femtoscopy [9]. At J-PARC, E27 collaboration reported a clear enhancement due to the “ ΣN cusp” in the inclusive missing-mass spectrum of the $d(\pi^+, K^+)$ reaction [10]. There exists a lot of experimental observations; however, the dynamical origin of the “ ΣN cusp” remains unclear as yet. One of the reasons is the resolution and statistics of the past experiments are not sufficient. In the proposed experiment, we aim to investigate the nature of “ ΣN cusp” with the world’s best resolution, 0.4 MeV in σ , and the high statistics more than 10^4 events.

In Sect. 1.1, the general explanation for the threshold cusp is described. In Sect. 1.2, the theoretical formula to express the “ ΣN cusp” in the proposed $d(K^-, \pi^-)$ reaction is shown. The detail of ΣN interaction and past experiments of the “ ΣN cusp” are described in Sect. 1.3 and 1.4, respectively.

1.1 Threshold cusp [11]

When a new threshold opens, it can make a cusp structure due to s -wave rescattering and its shape reflects the interaction in near-threshold region. Generally, two body scattering amplitude can be

expressed as,

$$T_L(E) \simeq 8\pi(m_1 + m_2) \frac{(2\mu E)^L}{1/A_L - i(\sqrt{2\mu E})^{2L+1}}, \quad (1)$$

where the m_1 and m_2 are the masses of the two particles and L is the orbital angular momentum [11]. Here, the relative momentum of the two particles k is approximated by the nonrelativistic expression $k \sim \sqrt{2\mu E}$ with the energy $E = \sqrt{s} - m_1 - m_2$ and the reduced mass $\mu = m_1 m_2 / (m_1 + m_2)$. From this equation, we can find that the first derivative with respect to E is discontinuous at the threshold for the s -wave. It can make the threshold cusp, while first derivative is continuous for the higher partial waves.

As expressed in Eq. (1), we can extract the information of the scattering length, A_L , from the cusp structure. Here, in this equation, only the scattering-length term is considered by the effective-range expansion because the relative momentum is small in near threshold region. It should be noted that the amplitude has a pole at $k = -i/A_0$. For large A_0 , the pole position is near the threshold and the pole seriously affects the experimental spectrum. Namely, the denominator of Eq. (1) is dominated by the $-i\sqrt{2\mu E}$ term and the cusp becomes evident. Therefore, the sharp cusp would hint at a near-threshold pole¹. On the other hand, for small A_0 , the pole position is far away from the threshold. In this case, the amplitude should behave rather smoothly because the denominator of Eq. (1) is dominated by the scattering length term which is constant.

Experimentally, a cusp-like structure was observed in the $\pi^0\pi^0$ invariant mass distribution from the $K^\pm \rightarrow \pi^\pm\pi^0\pi^0$ decay by the NA48/2 Collaboration [13, 14]. The significant structure appears at the $\pi^+\pi^-$ threshold and $\pi\pi$ s -wave scattering length was extracted from this structure. Analogously, it is suggested to extract $\pi\Sigma$ scattering length from the cusp structure of the $\Lambda_c \rightarrow \pi\pi\Sigma$ decay [15]. The measurement will be performed by the high luminosity Belle-II and BESIII experiments in near future. Moreover, the cusp structure was observed at \bar{K}^0n threshold in the $(K^-p \oplus K^+\bar{p})$ correlation function in high-energy pp collisions by ALICE Collaboration [16]. The measured spectrum was well described by the coupled-channel calculation with realistic potentials based on the chiral SU(3) dynamics [17].

1.2 Theoretical formula of the “ ΣN cusp” for the $K^-d \rightarrow \pi^- \Lambda p$ reaction [18]

Theoretical work for the “ ΣN cusp” was performed by Dalitz and Deloff [18, 19]. In the frame work of Ref. [18], the “ ΣN cusp” is generated through the following two-step processes,

$$K^- + d \rightarrow \pi^- + (\Sigma N)^+ \rightarrow \pi^- + \Lambda + p. \quad (2)$$

The reaction diagram is also shown in Fig. 1. In Ref. [18], the invariant mass spectrum of Λp pair, (= missing mass of $d(K^-, \pi^-)$ reaction), is estimated by adopting a zero-range central approximation for the two reactions $K^-N \rightarrow \pi^-\Sigma$ and $\Sigma N \rightarrow \Lambda p$.

The reaction amplitude for the net process shown in Eq. (2) can be expressed by three factors as,

$$T(\bar{K}d \rightarrow \pi\Lambda N) \sim T(\bar{K}N \rightarrow \pi\Sigma)F_d(Q_\Sigma, k_\Sigma)T(\Sigma N \rightarrow \Lambda N). \quad (3)$$

¹The threshold cusp may be possible to appear without near-threshold pole, called as Wigner-Baz’s cusp. However, the pure Wigner-Baz’s cusp (without near-threshold poles) should be only small effect, while the strong structure would appear when a near-threshold pole is present. Hence, the strong enhancements such as “ ΣN cusp” would be signals of the near-threshold pole. The detail is described in Sect. 2.1 of Ref [12].

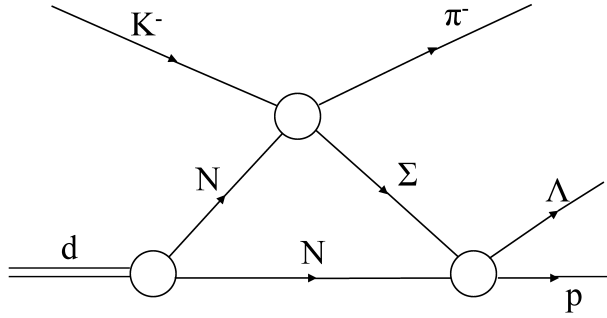


Figure 1: Reaction diagram of the “ ΣN cusp” for the $K^- d \rightarrow \pi^- \Lambda p$ reaction.

The first factor, $T(\bar{K}N \rightarrow \pi\Sigma)$, is T -matrix of the elementary process. The second one is deuteron factor reflecting the deuteron properties. It is given by

$$F_d(Q_\Sigma, k_\Sigma) = \int \frac{e^{ik_\Sigma r}}{r} e^{i\vec{Q}_\Sigma \cdot \vec{r}} \psi_d(r) d^3r \quad (4)$$

where \vec{Q}_Σ is expressed by the momentum transfer, \vec{q} , in the $K^- \rightarrow \pi^-$ transition and the masses as $\vec{Q}_\Sigma = \vec{q}m_N/(m_N + m_\Sigma)$. The k_Σ denotes the relative momentum of ΣN system in the final ΛN at rest frame. $\psi_d(r)$ denotes the deuteron wave function. The third factor, T -matrix of $\Sigma N \rightarrow \Lambda p$ process, is important term to describe the interaction of intermediate Σ particle with the second nucleon of the deuteron target.

For the (K^-, π^-) reaction at 0° , the amplitude of the elementary reaction $\bar{K}N \rightarrow \pi Y$ has no spin-flip component. Therefore, the YN states also are necessary to be in spin-triplet by reflecting the target-deuteron spin configuration. In practice, the experimental data spans a range of $\theta_{K\pi}$, but the angle are small enough, $\cos \theta_{CM} > 0.9$, and the spin-flip transition amplitude can be neglected. This is unique point for the $d(K^-, \pi^-)$ reaction. The other reactions not using deuteron target such as $pp \rightarrow K^+ \Lambda p$ reaction and Λp femtoscopy are difficult to extract only the spin-triplet component without spin observables.

In case of the (K^-, π^-) reaction at forward angles, the momentum transfer q is smaller and then the wavelength \hbar/q is comparable with the deuteron radius. In addition, the deuteron wavefunction is dominantly s -wave state. Therefore, the dominant transition induced by the small q is ${}^3S_1 \rightarrow {}^3S_1$ transition. As described in Sect. 1.1, the cusp is generated by the s -wave re-scattering. Moreover, since the measured final state is Λp , the total isospin of ΣN system should be $T = 1/2$.

Therefore, the third factor of Eq. (3), $T(\Sigma N \rightarrow \Lambda N)$, can be expressed in terms of the ΣN ($T = 1/2, {}^3S_1$) scattering length $A_0 = (a + ib)$ as follows²,

$$T(\Sigma N \rightarrow \Lambda N) \sim T_S^t(\Sigma N \rightarrow \Lambda N) = \frac{\beta_{\Sigma\Lambda}^t}{1 - ik_\Sigma A_0}, \quad (5)$$

where $\beta_{\Sigma\Lambda}^t$ is the $\Sigma N \rightarrow \Lambda N$ element of the reaction matrix and b is proportional to $(\beta_{\Sigma\Lambda}^t)^2$ (ΛN phase space). Note that it is clear that the reaction amplitude has a pole at $k_\Sigma = -i/A_0$ as same

²In this definition, the scattering length is attractive for $\text{Re}(A_0) > 0$.

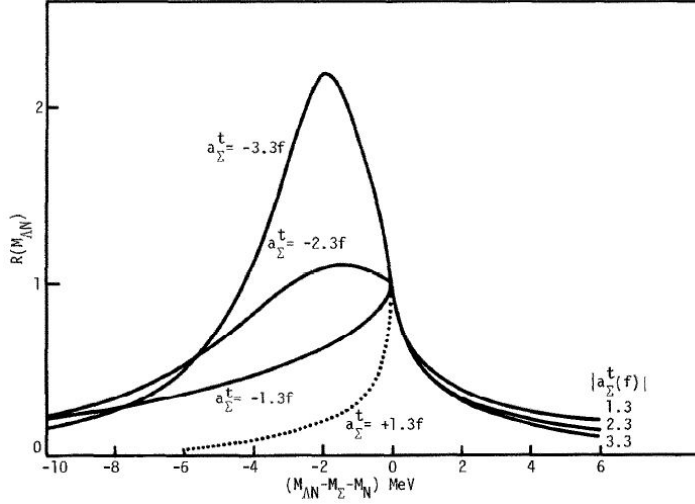


Figure 2: The product $|F_d(q, k_\Sigma)|^2 R_s^t$ as function of energy $M_{\Lambda N} - M_\Sigma - M_N$ which is taken from Ref. [18]. The cases of four choices of a with $b = 1.8$ fm are shown.

as Eq. (1) for $L = 0$. Then, above the threshold, the reaction rate related to $T(\Sigma N \rightarrow \Lambda N)$ term can be expressed as,

$$R_S^t \sim (k_\Sigma \sigma_S^t(\Sigma N \rightarrow \Lambda N)) = \frac{4\pi b}{(1 + k_\Sigma b)^2 + (k_\Sigma a)^2}. \quad (6)$$

Below the threshold, k_Σ is replaced by $+i|k_\Sigma|$ due to the analytic continuation, and the corresponding reaction rate is given by

$$R_S^t \sim \frac{4\pi b}{(1 + |k_\Sigma|a)^2 + k_\Sigma^2 b^2}. \quad (7)$$

Here, this expression is insensitive to a just above the threshold and does not depend on its sign there. The reaction rate falls rapidly just above the threshold because b should be positive and $k_\Sigma = \sqrt{2\mu E}$. Note that the reaction rate is almost entirely controlled by b (a) above (below) threshold.

The product of two factors R_s^t and $|F_d(q, k_\Sigma)|^2$ as function of the energy, which is proportional to the double differential cross section ($d^2\sigma/d\Omega/dE$), is shown in Fig. 2. This figure is taken from Ref. [18] and the spectra with four choices of a with $b = 1.8$ fm are demonstrated. As shown in the figure, the spectrum strongly depends on the scattering length. For example, the cusp shape is seen for $a = +1.3$ fm, where the pole exists in the third quadrant of k_Σ corresponding to “inelastic virtual state” [20]. A structure like the Breit-Wigner distribution can be found for $a = -3.3$ fm, where the pole position is second quadrant of k_Σ corresponding to “unstable bound state” [20]. Note that the higher partial waves $L > 0$ do not give rise to such a cusp.

In Ref. [18], they first consider the limit of charge independence, where two thresholds coincide ($\Sigma^+n = 2128.9$ MeV/ c^2 and $\Sigma^0p = 2130.9$ MeV/ c^2). Their separation, 2.0 MeV/ c^2 , may be better to be treated correctly [12, 19, 21]. To provide a simple illustration, we also do not consider the 2.0 MeV/ c^2 threshold difference in this proposal. We only consider the Σ^+n channel in the following

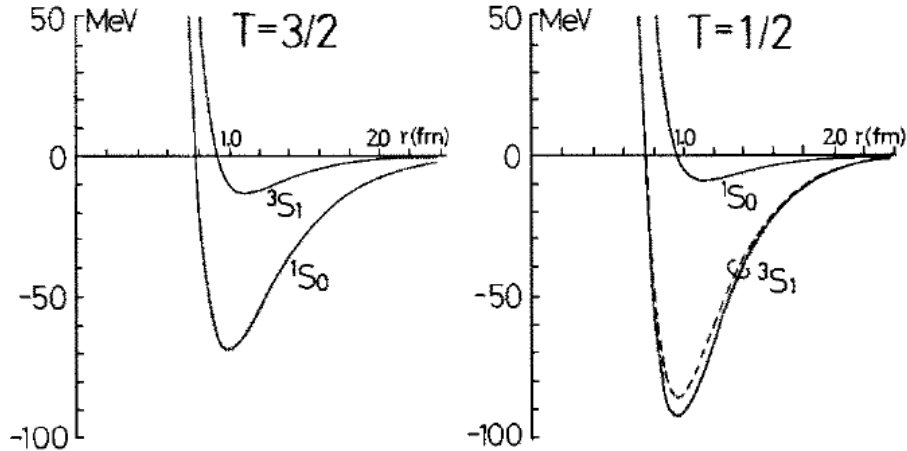


Figure 3: (a) The real parts of the ΣN potential for two body ΣN isospin(T)–spin(S) states $(T, S) = (3/2, 0), (3/2, 1), (1/2, 1),$ and $(1/2, 0)$ constructed by Harada *et al.*. This figure is taken from Ref. [23].

discussion for the simplicity. Indeed, the $\Sigma^0 p$ contribution would be less attribute due to the weight originated by the Clebsh-Golden coefficient [21].

1.3 ΣN interaction

As described in Sect. 1.2, the shape of “ ΣN cusp” would be affected by the ΣN interaction, especially scattering length. In this subsection, we describe the reviews of the ΣN interaction, especially for the $(T, S) = (1/2, 1)$ channel.

The ΣN interaction has recently studied via high-statistics $\Sigma^+ p$ and $\Sigma^- p$ scattering experiment (J-PARC E40) [22]. This experiment will make a great contribution to construct the realistic YN interaction models. However, in this type of experiment, ΣN scattering cross sections at very low energy ($p_Y^{lab} < 400$ MeV/ c), the region of s -wave dominance, are difficult to be measured. Moreover, the YN scattering data gives us only the spin average $\frac{1}{4}(3\sigma(S=1) + \sigma(S=0))$ of their cross sections. On the other hand, the proposed experiment can provide dedicated information of ΣN scattering length with isospin $T = 1/2$ and spin triplet channel as described in Sect. 1.2.

In the theoretical studies, Harada *et al.* constructed complex ΣN potentials assuming a simple two-range gaussian [23]. The potentials are constructed to be S -matrix equivalent to the meson exchange potential (Nijmegen model-D [24]). The ΣN interaction has the strong isospin–spin dependence as shown in Fig. 3. The attraction is stronger in the $(T, S) = (1/2, 1)$ and $(3/2, 0)$ channels compared with the other two channels. This characteristic feature is consistent with the comprehension of the quark-cluster model of baryon–baryon interaction developed by Oka *et al.* [25]. In this model, the strong repulsion is predicted in the $(T, S) = (1/2, 0)$ and $(3/2, 1)$ channels due to the quark Pauli principle. Moreover, the tendency of the isospin–spin dependence is also consistent with recent Lattice QCD calculation [26]. This isospin–spin dependence is a key to understand Σ -hypernuclei, especially in $A = 4$ system. Namely, the bound state was not observed in ${}^4\text{He}(K^-, \pi^+)$ spectrum but ${}^4\text{He}(K^-, \pi^-)$ spectrum [27] due to the strong isospin–spin dependence. See Appendix for the details.

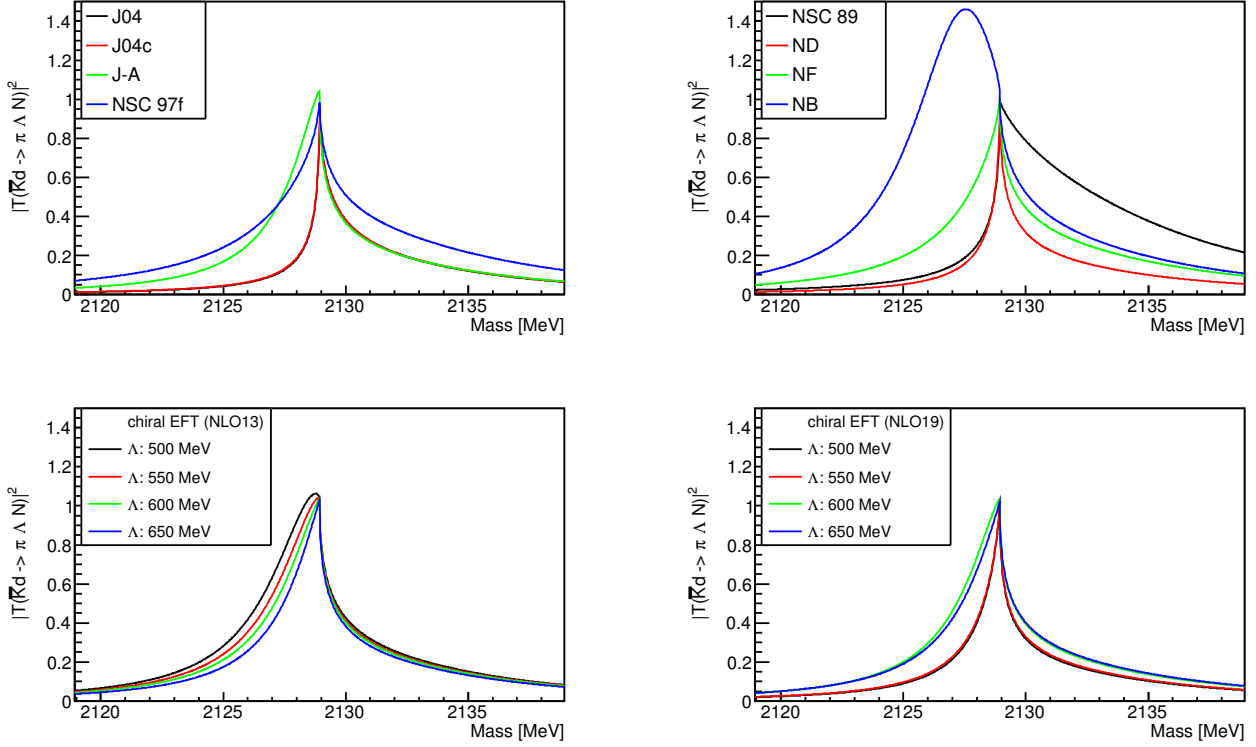


Figure 4: The calculated cusp spectra by the Eqs. (3)–(7) using the scattering-length values listed in Table 1. The vertical axis is normalized to be 1 at the Σ^+n threshold (2128.9 MeV).

Table 1: The summary of predicted ΣN scattering length in the $(T, S) = (1/2, 1)$ channel, $A_0 = a + ib$, by the various theoretical models [18, 20, 28, 29]. In case of the chiral EFT, the scattering length for each cutoff value, Λ , is shown in the table.

Model	J04	J04c	J-A	NSC 97f	NSC 89	ND	NF	NB
a [fm]	3.83	3.63	-2.37	-1.03	2.54	2.06	-1.29	-3.0
b [fm]	3.01	3.09	3.74	2.41	0.26	4.64	3.02	1.8
Model	chiral EFT (NLO13)				chiral EFT (NLO19)			
Λ [MeV]	500	550	600	650	500	550	600	650
a [fm]	-2.61	-2.44	-2.27	-2.06	-0.95	-0.98	-2.29	-1.95
b [fm]	2.89	3.11	3.29	3.59	4.77	4.59	3.39	3.38

As shown in Fig. 3, the ΣN potential in the $(T, S) = (1/2, 1)$ channel has a deep attractive pocket that may produce the ΣN bound state. The presence of a pole (bound or virtual) enhances the “ ΣN cusp” structure at the threshold. The consensus of the past investigations is that there exists a pole not far from the ΣN threshold, while the location of the pole position is not clear yet [18].

In Table 1, the predicted ΣN scattering length in the $(T, S) = (1/2, 1)$ channel by the various theoretical models are summarized. J04, J04c and J-A are the Jülich potentials taken from Ref. [28]. The values of NSC 97f, NSC 89, and Nijmegen model-D and F (ND and NF) are given from the pole positions in the complex k -plane, listed in Ref. [20], following the $k = -i/A_0$ relation. NB, Nijmegen model-B, is taken from Ref. [18]. Moreover, the scattering length obtained by the chiral effective theory (chiral EFT) is also listed taken from Ref. [29]. Here, the values with two versions, NLO13 and NLO19, and the different cutoff values (Λ) are shown in the table. The calculated spectra based on these theoretical values following Eqs. (3)–(7) are summarized in Fig. 4. As shown in the figure, the calculated shape strongly depends on the scattering length. By fitting the measured spectrum with the calculation, we will deduce the scattering length. It is also interesting to compare the measured spectrum with the calculations including the higher order terms given by the theoretical models, and then we can constrain them.

1.4 “ ΣN cusp” past experiments

The first experimental evidence of the “ ΣN cusp” was observed in $K^-d \rightarrow \pi^- \Lambda p$ reaction at rest more than 50 years ago [1]. An enhancement near the ΣN threshold ($\sim 2.13 \text{ GeV}/c^2$) was clearly observed in the Λp invariant-mass spectrum. This enhancement was confirmed by various experiments using $K^-d \rightarrow \pi^- \Lambda p$, $\pi^+d \rightarrow K^+ \Lambda p$, and $pp \rightarrow K^+ \Lambda p$ reactions [2, 3, 4, 5, 6, 7, 8]. These results were summarized in Ref. [30]. Moreover, the “ ΣN cusp” has also been observed by the Λ - p femtoscopy recently [9]. At J-PARC, E27 collaboration measured the “ ΣN cusp” in the inclusive missing-mass spectrum in the $d(\pi^+, K^+)$ reaction [10].

In Ref. [30], the spectra of the past experiments were reanalyzed by fitting with a Breit-Wigner function after subtracting the continuum background. The obtained peak positions and widths were compared as shown in Fig. 5. While the simple Breit-Wigner function (Lorentzian function) should not be suitable for the cusp as described in Sect. 1.1, the obtained peak position and width are not consistent with each other. They also tried to fit with two Breit-Wigner functions because a shoulder at about 10 MeV higher mass could be seen in several data. The results of the two Breit-Wigner fit are summarized in Fig. 6. There also exists the discrepancy of the peak position and width.

Here, we discuss the sensitivity of the past experiments. We summarize the characteristics of the past experiments in Table 2. “Tan” [5], which was bubble chamber experiment, measured the Λp invariant-mass in the stopped K^- reaction with better resolution, 1 MeV, compared to the other past experiments. It has clear enhancement near the ΣN threshold and the statistics was better than the other bubble chamber experiments. However, it is pointed out that the stopped K^- reaction has a difficulty to extract the ΣN scattering length from their spectra [19, 31, 32]. The formula described in Sect. 1.2 is based on the impulse approximation and this approximation can not be applied to at-rest or in-flight reaction with low beam momentum ($p_{beam} < 200 \text{ MeV}/c$). In case of at-rest reaction, multiple \bar{K} -scattering effect should be large and it can crucially distort the initial wave function. Especially, it is well known that the $\bar{K}N$ s -wave interaction with isospin

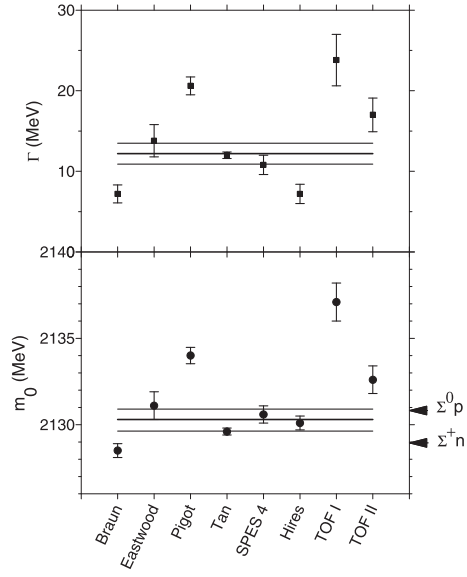


Figure 5: A summary of the peak positions (m_0) and widths (Γ) of one Breit-Wigner function taken from Ref. [30]. The fitting was done by the author of Ref. [30]. The values for the data set from Braun *et al.* [2], Eastwood *et al.* [3], Pigot *et al.* [4], Tan [5], SPES4 [6], HIREs [7], and TOF [8] are shown. The lines show the mean (thick line) and variance (thin line). The arrows show the thresholds of ΣN system.

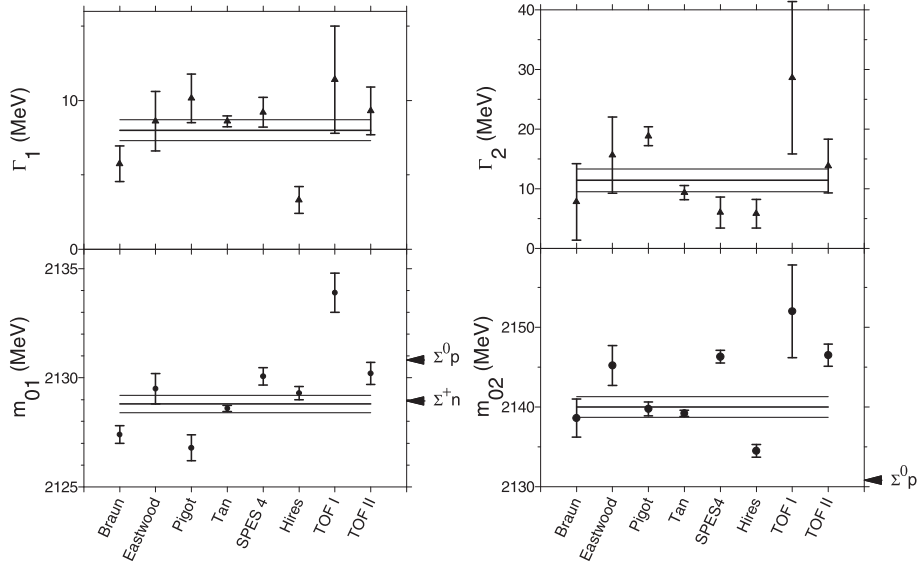


Figure 6: A summary of the peak positions (m_{01} , m_{02}) and widths (Γ_1 , Γ_2) of two Breit-Wigner functions taken from Ref. [30]. The fitting was done by the author of Ref. [30]. The used data sets are same as Fig. 5. The lines show the mean (thick line) and variance (thin line). The arrows show the thresholds of ΣN system.

Table 2: Summary of the past experiments. The references are Braun [2], Eastwood [3], Tan [5], Pigot [4], ALICE [9], and J-PARC E27 [10].

	Reaction	Comments	Statistics	Resolution	
Bubble chamber	Braun	Inflight $d(K^-, \pi^-) \Lambda p$ 680 – 840 MeV/c	Low statistic, worse resolution	603 events ($\cos \theta > 0.9$, momcut)	2 MeV
	Eastwood	Inflight $d(K^-, \pi^-) \Lambda p$ 1450, 1650 MeV/c	Low statistic worse resolution	217 events ($\cos \theta > 0.9$, momcut)	3 MeV
	Tan	stopped $d(K^-, \pi^-) \Lambda p$	Large FSI	2470 events	1 MeV
	Pigot	Inflight $d(K^-, \pi^-), d(\pi^+, K^+)$	Poor resolution	Uncertain	9.1 MeV ($d(K^-, \pi^-)$ 1.4 GeV/c)
	$pp \rightarrow \Lambda p K^+$ (COSY etc)	$pp \rightarrow \Lambda p K^+$	$^1S_0 + ^1S_3$ admixture Worse SN	High	0.8 MeV
	ALICE	pp (Femtoscopy)	$^1S_0 + ^1S_3$ admixture	High	No description
	J-PARC E27	$d(\pi^+, K^+)$ (Inclusive)	Worse SN (inclusive)	High	1.4 MeV

$T = 0$ gives strong scattering. On the other hand, the multiple \bar{K} -scattering effects are believed to be small, especially for a deuteron target, for the intermediate beam momenta of order 1 GeV/c. Moreover, the momentum of outgoing π^- of at-rest reaction is small, which is comparable with k_Σ . Hence, the final state interaction (FSI) between $\pi\Lambda$ and/or πN should also be crucial. Especially, there exists the resonance, $\Sigma(1385)$, strongly couples to $\pi\Lambda$, and its effect was clearly seen as shown in Fig.7(b) [1]. On the other hand, the momentum of outgoing π^- is much higher than k_Σ for the in-flight reaction with order of 1 GeV/c beam momentum and the FSI between $\pi\Lambda$ and πN should be small. Thus, the in-flight reaction is much simpler than the at-rest reaction theoretically.

“Braun” [2] and “Eastwood” [3] used the in-flight $K^-d \rightarrow \pi^- \Lambda p$ reaction at 680–840 and (1450 and 1650) MeV/c, respectively. They were also bubble chamber experiments. Their measured spectra are shown in Fig. 8. In the analysis, they chose forward scattering-angles, $\cos \theta_{K\pi(CM)} > 0.9$, to select low momentum-transfer events. Indeed, the enhancement due to the “ ΣN cusp” was invisible for the backward events, $0.8 < \cos \theta_{K\pi(CM)} < 0.9$ [2]. Moreover, in order to suppress the quasi-free (QF) back-ground events, they applied lower cutoff on the proton momentum in the final state. Then, they were able to exclude most of the genuine spectator events. By applying these forward scattering and proton momentum cut, a good signal-to-noise ratio was achieved as shown in Fig. 8. Especially, the spectrum of “Eastwood”, whose beam momenta are 1450 and 1650 MeV/c, looks almost background free. This is also the unique point to use the in-flight $K^-d \rightarrow \pi^- \Lambda p$ reaction. However, these experiments gave low statistics and worse resolutions. Only 603 (Braun) and 217 (Eastwood) events were remained after these event selection. The experimental resolutions were 2 MeV (Braun) and 3 MeV (Eastwood), it is difficult to discuss the original cusp shape with these resolutions. The characteristic cusp shape should be distorted by the experimental resolution, as demonstrated in Sect. 4.

“Pigot” *et al.* [4] measured the “ ΣN cusp” by using both $d(K^-, \pi^-)$ and $d(\pi^+, K^+)$ reactions at several beam momenta. They used the magnetic spectrometer system (counter experiment), however their mass resolution was quite bad (9 MeV for the $d(K^-, \pi^-)$ at 1.4 GeV/c). Such a bad resolution makes it quite difficult to discuss the cusp shape.

The “ ΣN cusp” was also observed in the $pp \rightarrow \Lambda p K^+$ reaction [6, 7, 8]. The best resolution for the “ ΣN cusp”, 0.8 MeV, was achieved by the COSY HIRES experiment [7] using this reaction.

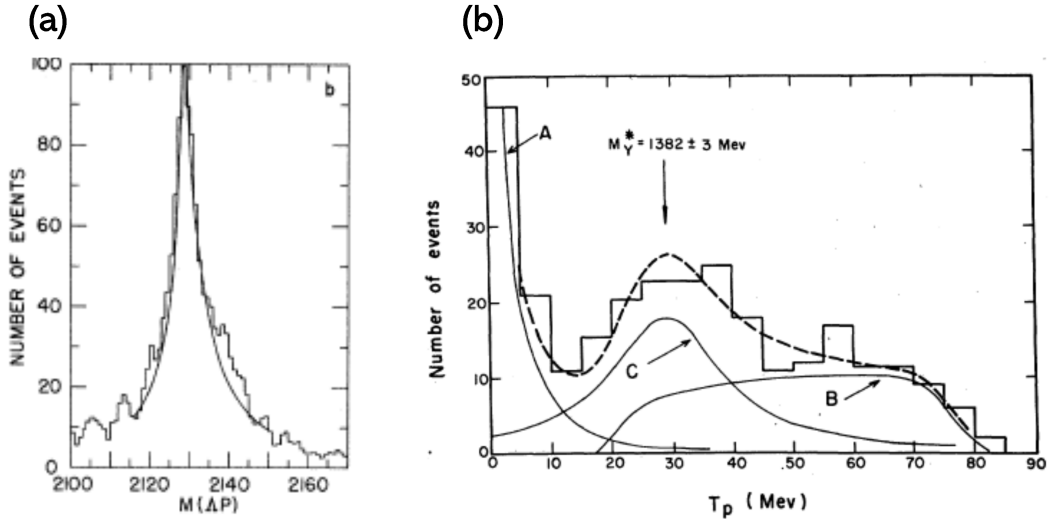


Figure 7: (a) The Λp invariant mass distribution of “Tan”, taken from [5]. (b) The kinetic energy distribution of proton in the $K^- d \rightarrow \pi^- \Lambda p$ reaction at rest, taken from [1]. The contribution of $\Sigma(1385)$ resonance, $\Sigma(1385) \rightarrow \Lambda \pi$, is clearly seen around the arrow in the figure.

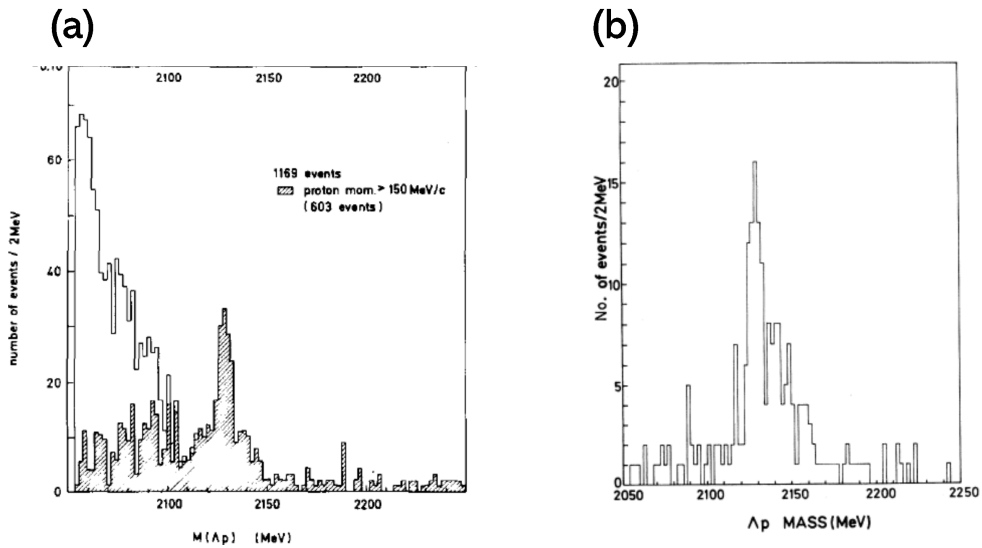


Figure 8: (a) The Λp invariant mass distribution of “Braun”, taken from [2]. In this spectra, the forward scattering angle, $\cos(\theta_{K\pi(CM)}) > 0.9$, is chosen. The shaded distribution shows the events with the proton momentum higher than 150 MeV/c. (b) The Λp invariant mass distribution of “Eastwood”, taken from [3]. The forward scattering angle, $\cos(\theta_{K\pi(CM)}) > 0.9$, and high momentum proton, ≥ 170 MeV/c, are selected.

The statistics were higher than old bubble chamber experiments. However, in this reaction, the signal-to-noise ratio is worse and the reaction mechanism is complicated. It is well known that the contribution of resonance door-way reactions via N^* and Δ^* are large. Moreover, the spin 1S_0 and 3S_1 components should be mixed in their spectra. The partial-wave analysis with spin observables are essential to understand the reaction mechanism and decompose 1S_0 and 3S_1 states in the pp reaction.

The recent femtoscopy by ALICE [9] can also give the important information for the ΣN interaction. However, there should exist both 1S_0 and 3S_1 components in the correlation spectrum. More complicated analysis with spin observables should be necessary to decompose each spin state. Future experiments using the $pp \rightarrow \Lambda p K^+$ reactions and the femtoscopy, with spin observables, may be competitors for the proposed experiment. Note that we can use the deuteron property to extract only the 3S_1 component as described in Sect. 1.2. It is quite unique point comparing the other reactions.

The J-PARC E27 also measured the “ ΣN cusp” by using the $d(\pi^+, K^+)$ reaction at 1.69 GeV/c. The statistics were high because it was counter experiment and the experimental resolution was 1.4 MeV. However, the signal-to-noise ratio was not good because they measured inclusive spectrum without final-state selection. The large quasi-free hyperon-production backgrounds were remained in their spectrum. Here, the same argument to extract the 3S_1 component can be applied for the $d(\pi^+, K^+)$ reaction. However, the momentum transfer of the (π^+, K^+) reaction is larger than that of (K^-, π^-) reaction. The cross section of “ ΣN cusp” in the (π^+, K^+) reaction is one order smaller than that of (K^-, π^-) reaction. Therefore, we conclude the $d(K^-, \pi^-)$ reaction is suitable for the “ ΣN cusp” experiment.

Finally, Dalitz pointed out the importance to perform the counter experiment (not bubble chamber experiment) with the in-flight $d(K^-, \pi^-)$ reaction giving the high resolution and high statistics [31]. However, such a high resolution and high statistics experiment with this reaction has not been performed after the suggestion. J-PARC is a good facility to provide the high intensity K^- beam and K1.8 beamline and S-2S spectrometers have good momentum resolution. The proposed experiment can satisfy the requirements which suggested by Dalitz and show the world’s best experimental quality for the “ ΣN cusp”.

2 Purpose of the proposed experiment

The purpose of proposed experiment is summarized as following,

- Investigate the nature of “ ΣN cusp”.
- Deduce the scattering length of the ΣN system with $(T, S) = (1/2, 1)$ by fitting the obtained missing-mass spectrum in the $d(K^-, \pi^-)$ reaction.

Whether “ ΣN cusp” is really cusp (inelastic virtual state) or unstable bound state is the important question in the strangeness nuclear physics. The one of the important key to solve this question is to achieve excellent missing-mass resolution and high statistics. In the proposed experiment, we will be able to achieve the best resolution of 0.4 MeV in σ , which is two times better than the past experiment (HIRES at COSY [7]).

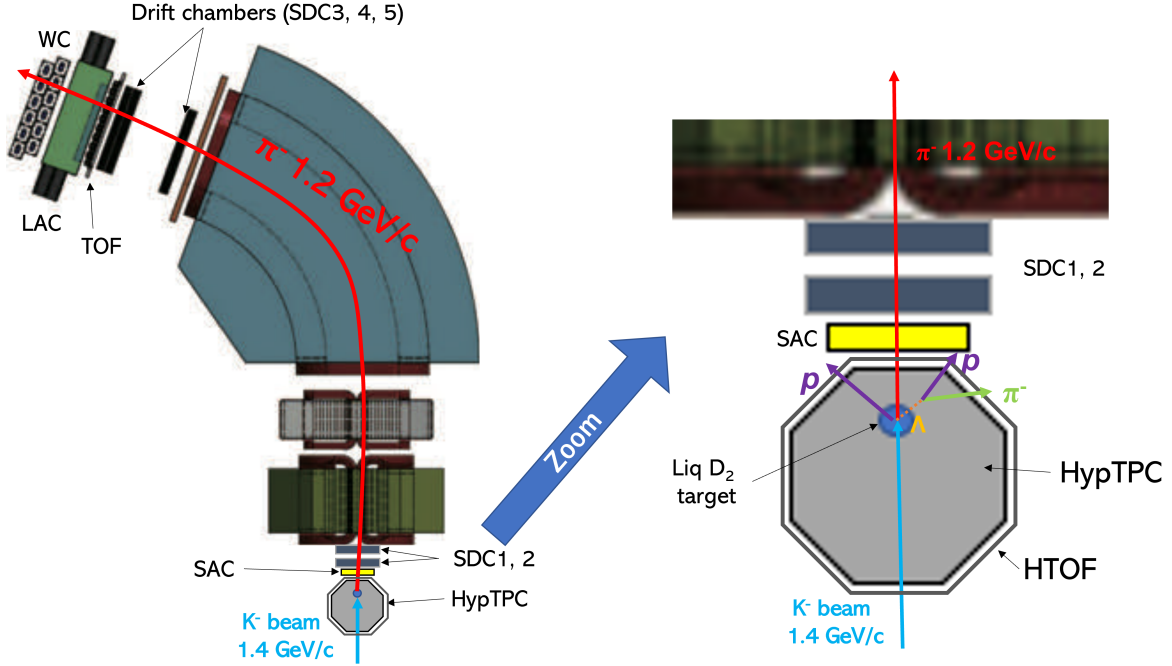


Figure 9: The schematic view of the proposed experiment.

3 Experimental Method

3.1 Setup

The proposed experiment will be performed at the K1.8 beam-line by using the S-2S spectrometer [33] and HypTPC [34]. Figure 9 shows the schematic view of the proposed experiment. The beam K^- will be measured by using the existing K1.8 beam-line spectrometer [35]. The momenta of beam particles can be reconstructed from the information of tracking detectors by using the third-order transfer matrix through the $QQDQQ$ system. The design value of the momentum resolution is $\delta p/p = 3.3 \times 10^{-4}$ (FWHM) with the position accuracy of 0.2 mm in rms.

The π^- scattered at the forward angles from the (K^-, π^-) reaction are momentum analyzed by using the S-2S spectrometer [33]. The momentum resolution of S-2S will be $\delta p/p = 6.0 \times 10^{-4}$ in FWHM. Then, the total mass resolution 0.4 MeV in σ will be achieved. Here, the energy-loss term is negligibly small because the target thickness is small, liquid deuterium 0.166 g/cm^3 with 54 mm ϕ . The S-2S is composed of drift chambers (SDCs), two quadrupole and one dipole magnets (QQD), time-of-flight scintillation counter (TOF), aerogel Čerenkov counter (LAC), and water Čerenkov counter (WC). The S-2S have the solid angle as large as 55 msr due to the large aperture of the two quadrupole magnets. Since S-2S spectrometer is designed to measure the scattered K^+ in the (K^-, K^+) reaction for the Ξ -hypernucleus search (E70 [33]), the water Čerenkov counter (WC) are installed to suppress the scattered proton events in the trigger level. The WC will not be used as the trigger counter because we need to measure the scattered π^- . The aerogel Čerenkov counter (SAC) will be additionally installed in front of the SDC1 as Fig. 9 to improve the scattered π^- selection quality. Then, the π^- trigger signals will be generated by using two aerogel Čerenkov

counters, SAC and LAC, time-of-flight scintillation counter (TOF), as $TOF \otimes SAC \otimes LAC$. The particle identification will be performed by combing the information of TOF, reconstructed flight path and momentum by the tracking in S-2S.

In the proposed experiment, we plan to install the Time Projection Chamber (HypTPC) to suppress the quasi-free backgrounds and improve the signal-to-noise ratio. The detailed strategy to suppress the background by using HypTPC is described in Sect. 3.3. The liquid deuterium target will be installed inside the TPC volume to achieve the large acceptance. We plan to use the same liquid target system as J-PARC E45 experiment, which is the baryon spectroscopy using the $p(\pi^\pm, 2\pi)$ reaction. The liquid target has a vertical cylindrical cell with the dimensions of 54 mm diameter and 100 mm length to fill LH_2 or LD_2 . In this liquid target system, there exists the material budget around the target such as G10-target holder (3 mm thick) and GRRP target vacuum cylinder (1.5 mm thick). The detailed information of the liquid target system is described in Technical Design Report of E45 experiment [36].

The HypTPC was developed for the H-dibryon search experiment called as J-PARC E42 [37], which was successfully finished the data taking in June 2021. In order to operate the TPC under the high particle-rate condition, we adopt the triple GEMs (Gas Electron Multiplier) amplification for the signal detection and the gating-wire grid to suppress the ion back-flow. Moreover, the P-10 (Ar-CH4 (90:10)) gas, whose maximum drift velocity is 5.3 cm/s, is selected for the high particle-rate capability. The signal, which is amplified by the triple GEMs, is read out by the concentric anode-pad plane. The readout-pad configuration has been optimized for spatial resolution to be 0.2–0.3 mm at the gas gain of 10^4 . The inner sector has 10 radial pad rows with pads of 9 mm in length and 2.1–2.7 mm in width, and the outer sector has 22 pad rows with pads of 12.5 mm in length and 2.3–2.4 mm width, resulting in a total of 5768 pads.

Usually, HypTPC is installed inside the superconducting dipole magnet to measure the momentum of the charge particles from their trajectories. In the proposed experiment, we will not use the magnet due to the space limitation of S-2S. We need to put the experimental target, liquid deuterium target, near the S-2S in order to achieve the reasonable acceptance for the scattered π^- . Here, the distance between SDC1 and experimental target in E70 is about 10 cm. Moreover, the HypTPC will be rotated 180 degree in the beam axis for this requirement. In the original configuration of HypTPC such as E42, the experimental target is positioned 143 mm upstream, however it will be downstream as shown in Fig. 9. The charged particle trajectory of the (K^-, π^-) reaction and decay products will be tracked by HypTPC. Moreover, the time-of-flight of the decay products can be measure by the plastic scintillation counters, HTOF, which surrounds HypTPC.

3.2 Yield estimation

The yield (per day) of the “ ΣN cusp” in the inclusive measurement is estimated in the following way:

$$N = \left(\frac{d\sigma}{d\Omega}\right) \times d\Omega_{S2S} \times \left(\frac{N_{beam} \times N_A \times (\rho x)}{A}\right) \times \epsilon. \quad (8)$$

$\left(\frac{d\sigma}{d\Omega}\right)$ is the differential cross section of the “ ΣN cusp”, which is deduced as $127 \mu\text{b}/\text{sr}$ in the laboratory system from the measurement of “Eastwood” [3]. $d\Omega_{S2S} = 50 \text{ msr}$, is the acceptance of S-2S for the π^- detection. N_{beam} is the number of beam kaons assuming the beam intensity as $0.5 \times 10^6 K^-/\text{spill}$, where 1 spill is assumed to be 4 seconds, and accelerator efficiency as 0.9. N_A is the Avogadro’s number and $A = 2$ is the mass number of the target nucleus. (ρx) is the effective

target-thickness estimated to be 0.54 g/cm^2 by taking into account the beam size, $\sigma_x \sim 2.3 \text{ cm}$, and target dimension, $\phi = 5.3 \text{ cm}$. ϵ is the overall efficiency (DAQ, analysis, decay in flight of π^- , etc.), assumed to be 0.5.

In total, about 7.6×10^4 events of the “ ΣN cusp” is expected in the inclusive measurement in the 15 days beam-time. In the coincidence measurement, we also need to consider the detection efficiency of decay products by HypTPC (ϵ_{HypTPC}) which is estimated to be 0.2, where the detail of background suppression by HypTPC is described in Sect. 3.3. Then, 1.4×10^4 events of the “ ΣN cusp” will be measured in the coincidence analysis with HypTPC in the 15 days beam-time. This statistics is one order higher than the old bubble chamber experiments. The order of 1×10^4 events statistics is necessary for the finite shape fitting.

3.3 Quasi-free background suppression by HypTPC

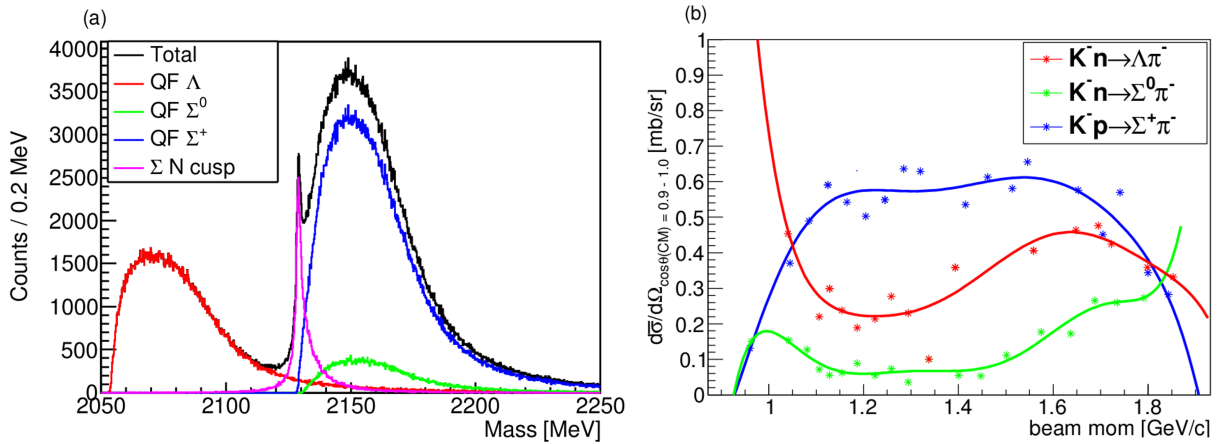


Figure 10: (a) The expected inclusive missing-mass spectrum of the $d(K^-, \pi^-)$ reaction at 1.4 GeV/c with 15 days beam-time. The overall spectrum is shown by the black line. Each process is shown in the figure with different colors. (b) The elementary differential cross-section at the forward scattering angle, $\cos \theta_{CM} > 0.9$, as a function of K^- beam momentum. The values, which are shown by the points, are deduced from the bubble chamber measurements [38, 39, 40, 41, 42]. The lines indicate the results of polynomial fit of these data points to show the global tendency.

In the $d(K^-, \pi^-)$ reaction at 1.4 GeV/c, there are three quasi-free hyperon production processes as,

$$K^- \text{“}n\text{”} \rightarrow \Lambda \pi^-, \quad (9)$$

$$K^- \text{“}n\text{”} \rightarrow \Sigma^0 \pi^-, \quad (10)$$

$$K^- \text{“}p\text{”} \rightarrow \Sigma^+ \pi^-, \quad (11)$$

where “ n ” and “ p ” indicate the neutron and proton in the deuteron, respectively. Around the energy region of “ ΣN cusp”, these three quasi-free reactions are necessary to be considered as the background. The differential cross-section of elementary process has already been measured by the old bubble chamber experiments [38, 39, 40, 41, 42]. Figure. 10(a) shows the expected inclusive missing-mass spectrum of the $d(K^-, \pi^-)$ reaction at 1.4 GeV/c simulated based on these measured

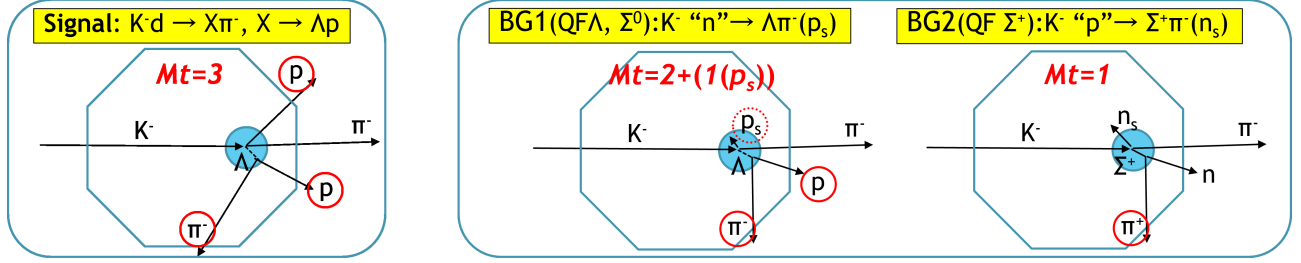


Figure 11: The schematic views of the background reduction selecting the multiplicity of charged particles by HypTPC. The schematic trajectory the “ ΣN cusp” process (Signal) is shown in left figure. The background schematic trajectory are shown in center and right figures. See the detail in the text.

elementary cross sections, as shown in Fig. 10(b), with a smearing by the nucleon Fermi-motion in deuteron [43]. The quasi-free Λ , Σ^0 , and Σ^+ components are shown by red, green, and blue lines, respectively. The “ ΣN cusp” contribution, where the detail of yield estimation is described in Sect. 3.2, is shown by the magenta line. The overall expected inclusive-spectrum corresponds to the black line. Here, the experimental resolution, $\sigma = 0.4$ MeV, is also considered in the simulation. As shown in this figure, the “ ΣN cusp” signal should be clearly seen in the inclusive spectrum due to the good energy resolution.

In the proposed experiment, we plan to suppress these quasi-free backgrounds by detecting the charged particle multiplicity with HypTPC. The coincidence spectrum will be mainly used to derive the scattering length from the “ ΣN cusp”, while the inclusive spectrum is also useful for the physics analysis. The schematic view of the background reduction by HypTPC is shown in Fig. 11. The schematic trajectory of the signal, “ ΣN cusp” process, is shown in the left figure. In the signal process, three charged particle (p , p , and π^-) can be produced as decay products as

$$K^- d \rightarrow X \pi^-, \quad X \rightarrow \Lambda p, \quad \Lambda \rightarrow p \pi^-, \quad (12)$$

where X corresponds to the “ ΣN cusp”. The measured charge multiplicity in HypTPC should be $Mt = 3$ because these three charged particles, which are enclosed with circles in Fig. 11, can have sufficient momentum to escape from the liquid target.

For the background, we categorize them into two processes as in BG1(QF Λ , Σ^0) and BG2(QF Σ^+) as shown in Fig. 11. In case of BG1, three charged particles (p , π^- , and p_s) can be produced as decay products as

$$K^- \text{“}n\text{”} \rightarrow \Lambda \pi^- p_s, \quad \Lambda \rightarrow p \pi^-, \quad (13)$$

$$K^- \text{“}n\text{”} \rightarrow \Sigma^0 \pi^- p_s, \quad \Sigma^0 \rightarrow \Lambda \gamma, \quad \Lambda \rightarrow p \pi^-, \quad (14)$$

where p_s indicates the spectator proton of the quasi-free process. However, the momentum of spectator proton should be small and almost all of the spectator proton will stop inside the target. Therefore, the measured charge multiplicity of the decay products should be mainly $Mt = 2$.

In case of BG2, only one charged particle (π^+ or p) can be produced as decay products as

$$K^- \text{“}p\text{”} \rightarrow \Sigma^+ \pi^- n_s, \quad \Sigma^+ \rightarrow n \pi^+ \quad \text{or} \quad p \pi^0, \quad (15)$$

where n_s is the spectator neutron of the quasi-free process. Then, BG2 is easier to be suppressed comparing BG1 by the charged multiplicity. Note that the Σ production as expressed in Eqs. (10)

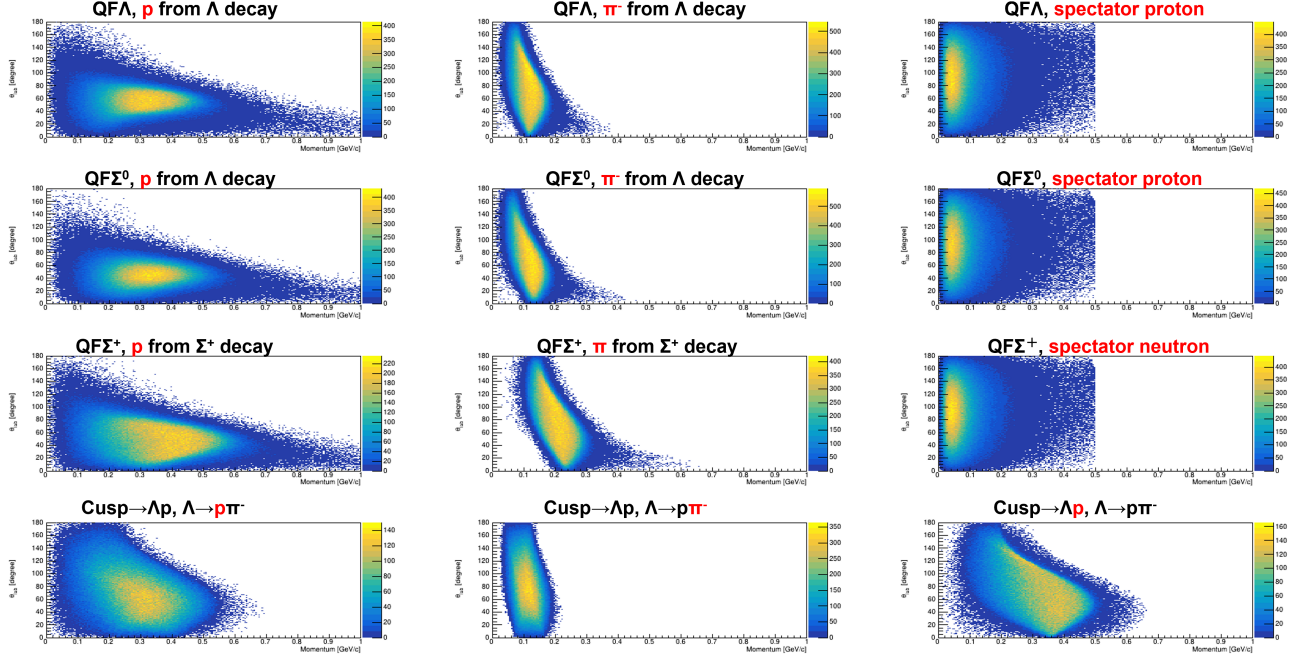


Figure 12: The simulated momentum and scattering angle, θ_{Lab} , distributions for the quasi-free backgrounds and “ ΣN cusp” reactions. The corresponding particles for each reaction is shown by the red character.

and (11) is the first step reaction of the “ ΣN cusp” production, as described in Sect. 1.2. Therefore, we need the large Σ production cross-section to have the large “ ΣN cusp” yield.

The elementary differential cross-section at the forward scattering angles, $\cos \theta_{CM} > 0.9$, as a function of K^- beam momentum is shown in Fig. 10(b). In order to achieve the good signal-to-noise ratio (SN ratio), it is better to select the beam momentum where the cross section of Σ^+ production is large and those of Λ and Σ^0 are small. Moreover, the higher beam momentum has an advantage to achieve the higher beam intensity to suppress the K^- decay in flight before the target. By considering them, we chose the 1.4 GeV/c as the beam momentum.

The simulated momentum, scattering angle θ in laboratory system, distributions of the decay products for the quasi-free backgrounds and “ ΣN cusp” are summarized in Fig. 12. The corresponding particles for each reaction is shown by the red character in the title for each spectrum. Note that, protons from the “ ΣN cusp” has higher momentum as $\gtrsim 200$ MeV/c. On the other hands, the momentum of spectator proton in the quasi-free background should be small $\lesssim 200$ MeV/c. The charged particles with low momentum should stop in the materials around the liquid target system and it can not be detected by HypTPC. Therefore, by requiring the multiplicity $Mt = 3$ in HypTPC, we can strongly suppress these quasi-free background as demonstrated in Fig. 13.

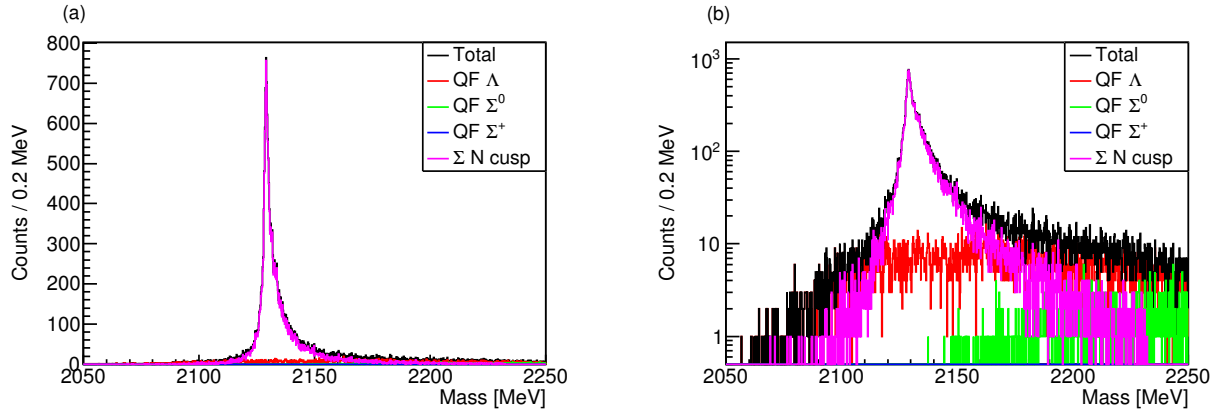


Figure 13: The simulated coincidence spectra by requiring the charged multiplicity $Mt = 3$ (without (K^-, π^-) measurements) with HypTPC. The overall spectrum is shown by the black lines and the sub components are displayed by the colored lines. The linear and semi-log plots are shown in (a) and (b), respectively.

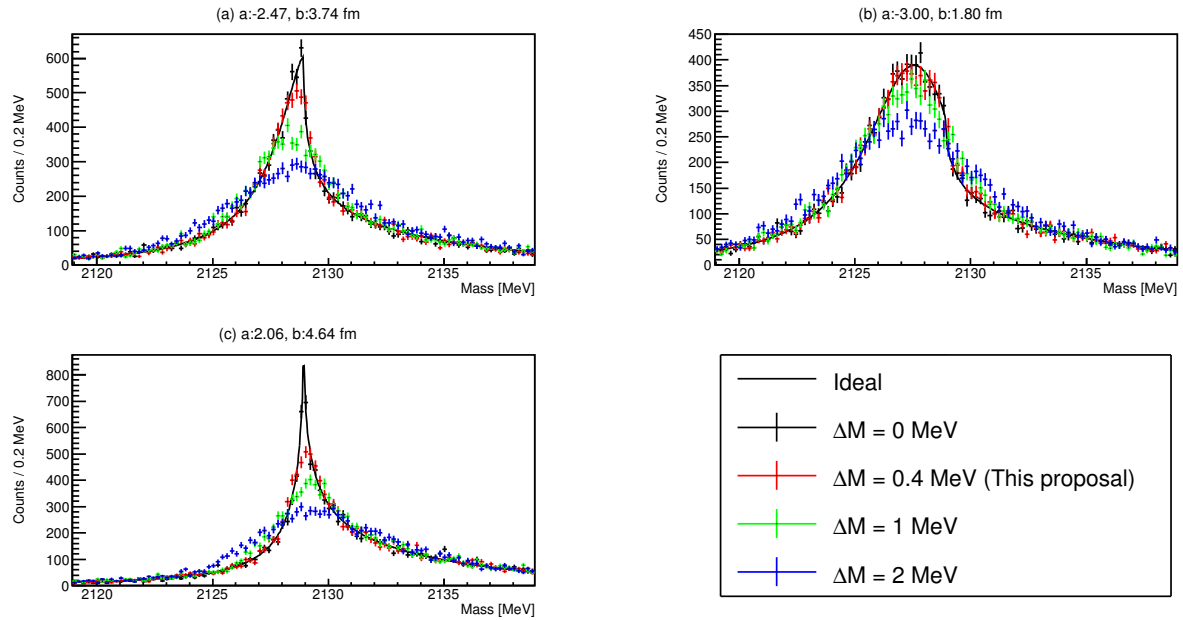


Figure 14: The simulated mass-distributions for several choice of scattering-length, which are shown in title in the figures. The solid black-lines show the original distribution given by the Eqs. (3)–(7). The points with error bars shows the smeared spectra with the experimental resolution of $\Delta M = 0, 0.4, 1,$ and 2 MeV in σ . The statistic errors with 1.4×10^4 events are also demonstrated in the spectra. The spectra are plotted by 0.2 MeV binning.

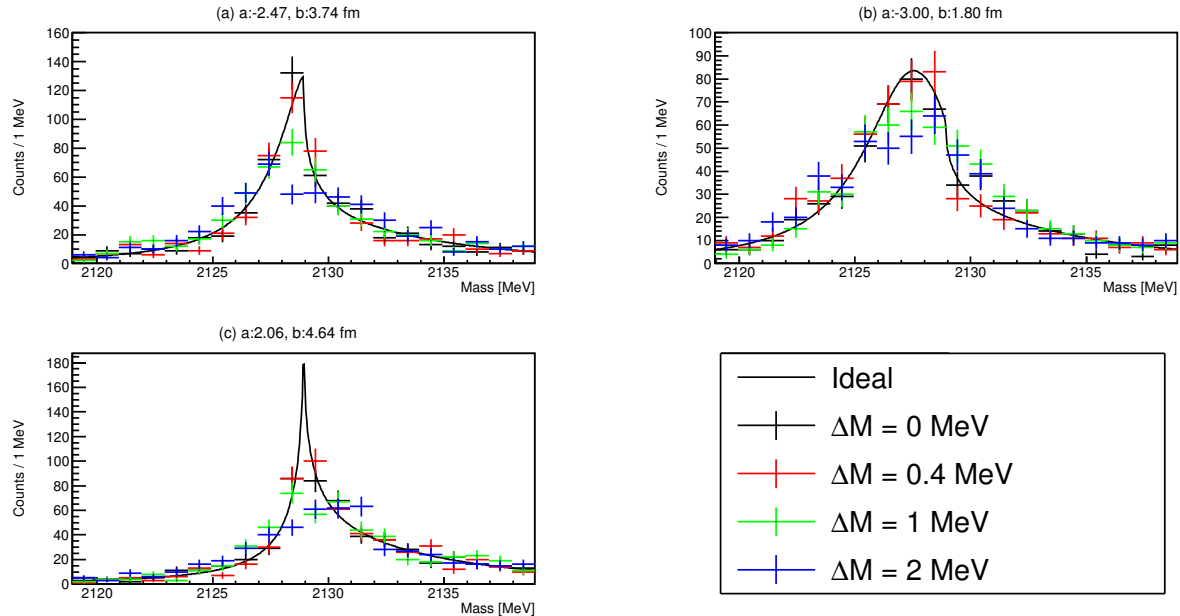


Figure 15: The same figures as Fig. 14, but with different statistics as 600 events, which corresponds to the old bubble-chamber experiment “Braun” [2]. The spectra are plotted by 1 MeV binning.

4 Expected result

The simulated missing-mass distributions are shown in Fig. 14. In these figures, 3 choices of scattering length are shown to demonstrate different shapes. Namely, the values of J-A ((a), shallow bound), NB ((b), deeply bound), and ND ((c), sharp cusp), whose values are summarized in Table 1, are chosen for the comparison. Note that there is no reason to select these three models by considering theoretical justification. The points with error bars are the smeared spectra with the experimental resolution of $\Delta M = 0, 0.4, 1,$ and 2 MeV in σ shown by the different colors. In these plots, 1.4×10^4 events, corresponding to the statistics for the proposed experiment, are generated and the statistical errors are shown in the figures.

Here, “Braun” [2] and “Eastwood” [3] are the past experiments using the in-flight $d(K^-, \pi^-)$ reaction, which can suppress the FSI between $\pi\Lambda$ and πN and choose 3S_1 spin states following the deuteron property as explained in Sect. 1.4. The mass resolutions of these experiments are 2 MeV (“Braun”) and 3 MeV (“Eastwood”). As shown in Fig. 14, the original shapes are significantly distorted in the case of $\Delta M = 2$ MeV. Moreover, the statistics of these past experiments are poor as 603 events (“Braun”) and 217 events (“Eastwood”) and the statistical effects are demonstrated in Fig. 15. In these old bubble chamber experiments, they plotted the obtained mass distributions with 1 MeV binning as shown in Fig. 8. However, finer binning is necessary to derive the original-mass distributions as shown in Fig. 14. For this purpose, we need the higher statistics more than 1×10^4 events and good resolution < 1 MeV.

The comparisons between the scattering-length fit and Breit-Wigner fit are demonstrated in Fig. 16. The data points are same as Fig. 14. The red lines show the results with the scattering-length fit, where the fitting function is same as the generated distributions. The green lines show

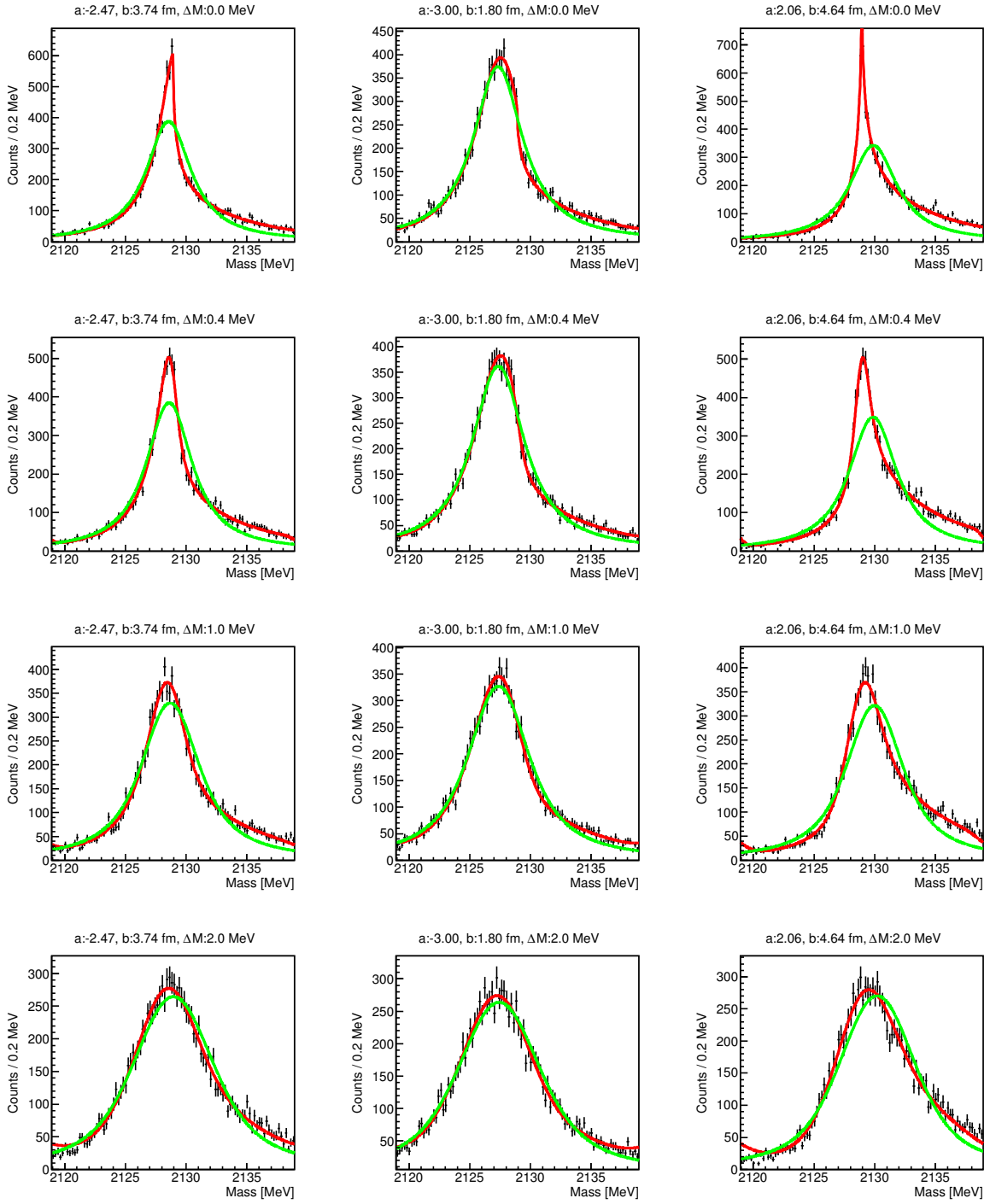


Figure 16: The comparison between the scattering-length fit and Breit-Wigner fit. See the detail in the text.

the simple Breit-Wigner (Lorentzian) fit results for the comparison. For both fits, the experimental resolution are convoluted to the fitting function. The scattering length and mass resolution are shown in the title of each spectrum.

As shown in the figures, fitting results with scattering-length formula (red curve) and Breit-Wigner (green curve) are almost the same in case of the worse resolution, $\Delta M = 2$ MeV. It is because the original shape is strongly distorted by the resolution. On the other hand, the clear difference between red and green curves can be seen in case of the present resolution, $\Delta M = 0.4$ MeV. Therefore, the high resolution is really important for the “ ΣN cusp” to distinguish the model function. From the fit of Fig. 16, we found that we can deduce the scattering length with the statistical error of $\lesssim 0.3$ fm. It is also important to compare the measured spectrum with the calculation including the higher order terms, such as effective range. In this case, we will not take into account them as the free parameter and input the given values by theoretical models. Similar attempts were made by the recent femptoscropy. Then, we can constrain the theoretical models. Finally, it should be noted that the high precision experimental data is essential to quantitatively discuss the pole position and extract the interaction strength.

5 Run plan and beam time request

We request 15 days for the physics run, based on yield estimation described in Sect. 3.2. In addition, we need the following beam times.

- 5 days for the empty target run.
- 1 day for the hydrogen target run.
- 3 days for the detector commissioning.

We need three days of beam tune and detector commissioning run. We request to take the empty target data to subtract the contribution of the K^- beam decay in-flight for the inclusive analysis. The empty target data is also useful to estimate the surrounding materials contribution in the liquid target system such as the target cell. The hydrogen target data will be taken for the calibration. The momentum correction will be performed by checking the missing mass of Σ^+ in the $K^- p \rightarrow \Sigma^+ \pi^-$ reaction. Moreover, the evaluated differential cross section of the Σ^+ production will be compared with the past experiment. The systematic error of the efficiency evaluation and effective target thickness will be discussed from the comparison.

We will use the S-2S spectrometer, whose construction is on-going for E70 experiment. HypTPC detector are common with E45 and E72 experiments. We need to newly develop the small aerogel Čerenkov counter (SAC), the detail is described in Sect. 3.1. Moreover, the support structures for HTOF and the liquid target system will be newly prepared for the proposed experiment because we will not use the HS magnet. We will be ready to start the proposed experiment by the end of FY2023 because the main detectors are common with the other J-PARC experiments.

6 Summary

We have proposed the high resolution missing-mass spectroscopy of the “ ΣN cusp” by using the S-2S spectrometer and HypTPC. The mass resolution is the quite important key to investigate the

nature of “ ΣN cusp”. We can achieve 0.4 MeV resolution in σ , which is two time better than the past experiment achieved by the COSY HIRES experiment [7]. Moreover, the in-flight $d(K^-, \pi^-)$ reaction is unique to derive 3S_1 spin contribution with low background. By fitting the measured mass spectra, we are able to deduce the ($T = 1/2, S = 1$) ΣN scattering length with the good accuracy, statistical error of $\lesssim 0.3$ fm.

Acknowledgements

We would like to thank the fruitful discussion regarding the “ ΣN cusp” with Prof. A. Hosaka, Dr. S. Sakai, Dr. Y. Yamaguchi, and Dr. D. Sombillo.

References

- [1] O.I. Dahl *et al.*, Phys. Rev. Lett., **6**, 3 (1961).
- [2] O. Braun *et al.*, Nucl. Phys. **B124**, 45 (1977).
- [3] D. Eastwood *et al.*, Phys. Rev. D **3**, 2603 (1971).
- [4] C. Pigot *et al.*, Nucl. Phys. **B249**, 172 (1985).
- [5] T.H. Tan, Phys. Rev. Lett. **23**, 395 (1969).
- [6] R. Siebert *et al.*, Nucl. Phys. **A567**, 819 (1994).
- [7] A. Budzanowski *et al.*, Phys. Lett. **B692**, 10 (2010).
- [8] S. Abd El-Samad *et al.*, Eur. Phys. J. A **49**, 41 (2013).
- [9] ALICE Collaboration, arXiv:2104.04427
- [10] Y. Ichikawa *et al.*, Prog. Theor. Exp. Phys. **2014**, 101D03 (2014).
- [11] F. Guo, X. Liu, and S. Sakai, Prog. Part. Nucl. Phys. **112**, 103757 (2020).
- [12] A.M. Badalian, L.P. Kok, M.I. Polikarpov, and Yu.A. Simonov, Phys. Rep. **82**, 31 (1982).
- [13] J.R. Batley *et al.*, Phys. Lett. **B633**, 173 (2006).
- [14] J.R. Batley *et al.*, Eur. Phys. J. **C64**, 589 (2009).
- [15] T. Hyodo and M. Oka, Phys. Rev. C **84**, 035201 (2011).
- [16] S. Acharya *et al.* (ALICE Collaboration), Phys. Rev. Lett **124**, 092301 (2020).
- [17] Y. Kamiya, T. Hyodo, K. Morita, A. Ohnishi, and W. Weise, Phys. Rev. Lett. **124**, 132501 (2020).
- [18] R.H. Dalitz, Nucl. Phys. **A354**, 101, (1981).
- [19] R.H. Dalitz and A. Deloff, Czech. J. Phys. **B**, 32, (1982).

- [20] K. Miyagawa and H. Yamamura, Phys. Rev. C **60**, 024003 (1999).
- [21] J.Haidenbauer and U.-G. Meißner, Chi. Phys. C **45**, 094104 (2020).
- [22] K. Miwa *et al.*, http://j-parc.jp/researcher/Hadron/en/pac_1101/pdf/KEK_J-PARC-PAC2010-12.pdf
K. Miwa *et al.*, Phys. Rev. C **104**, 045204 (2021).
- [23] T. Harada, S. Shinmura, Y. Akaishi and H. Tanaka, Nucl. Phys. **A507**, 715 (1990).
- [24] M.M. Nagels, T.A. Rijken, and J.J. de Swart Phys. Rev. D **20**, 1633 (1979).
- [25] M. Oka, K. Shimizu and K. Yazaki, Prog. Theor. Phys. Suppl. **137**, 1 (2000).
- [26] H. Nemura for the HAL QCD Collaboration, AIP Conf. Proc. **2130** (2019).
- [27] T. Nagae *et al.*, Phys. Rev. Lett. **80**, 1605 (1998).
- [28] J. Haidenbauer and Ulf-G. Meißner, Phys. Rev. C **72**, 044005 (2005).
- [29] J.Haidenbauer, U.-G. Meißner, and A. Nogga, Eur. Phys. J. A **56**, 3 (2020).
- [30] H. Machner *et al.*, Nucl. Phys. A **901**, 65 (2013).
- [31] R.H. Dalitz and A. Deloff, Aust. J. Phys. **36**, 617 (1983).
- [32] M. Torres, R.H. Dalitz and A. Deloff, Phys. Lett. **B 174**, 213 (1986).
- [33] T. Nagae *et al.*, http://j-parc.jp/researcher/Hadron/en/pac_1801/pdf/P70_2018-10.pdf
- [34] S.H. Kim *et al.*, Nucl. Instrum. Meth. A **940**, 359 (2019).
- [35] T. Takahashi (the Hadron Beamline Group and the K1.8 Experimental Group), Nucl. Phys. A **835**, 88 (2010).
- [36] Technical Design Report of J-PARC E45 experiment.
- [37] J.K. Ahn *et al.*, https://j-parc.jp/researcher/Hadron/en/pac_1201/pdf/KEK_J-PARC-PAC2011-06.pdf
- [38] B. Conforto *et al.*, Nucl. Phys. **B105**, 189 (1976).
- [39] A. Berthon *et al.*, Nucl. Phys. **B24**, 417 (1970).
- [40] M.J. Corden *et al.*, Nucl Phys. **B125**, 61 (1977).
- [41] M.J. Corden *et al.*, Nucl. Phys. **B153**, 485 (1979).
- [42] M.J. Corden *et al.*, Nucl. Phys. **B104**, 382 (1976).
- [43] R. Machleidt, K. Holinde and Ch. Elster, Phys. Rep. **149**, 1 (1987).

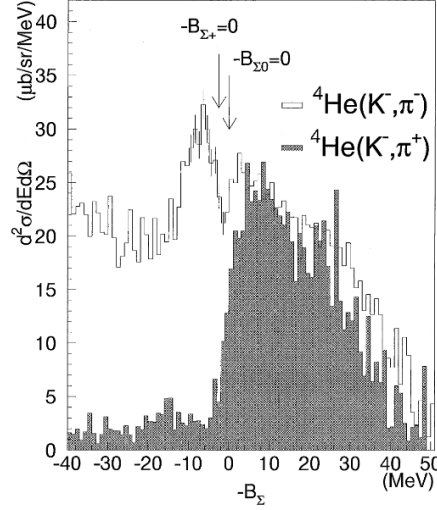


Figure 17: The excitation energy spectra of the ${}^4\text{He}(K^-, \pi^-)$ and ${}^4\text{He}(K^-, \pi^+)$ reaction measured by the BNL E905 experiment. The binding energy threshold was determined by Σ^0 production for the (K^-, π^-) reaction, and that of the Σ^- production for the (K^-, π^+) reaction. This figure is taken from Ref. [27].

Appendix

A ${}^4_{\Sigma}\text{He}$ and spin–isospin dependence of the ΣN interaction

Through s -shell and p -shell Σ -hypernucleus studies, only the ${}^4_{\Sigma}\text{He}$ bound state was observed. The BNL E905 experiment was performed by using the in-flight (K^-, π^{\pm}) reaction on the liquid ${}^4\text{He}$ target [27]. They found the bound state peak in the (K^-, π^-) spectrum and almost no event below the Σ binding threshold in the (K^-, π^+) spectrum as shown in Fig. 17. By considering the difference between (K^-, π^-) and (K^-, π^+) spectra, it can be interpreted that the Σ -nucleus potential strongly depends on the total isospin T . In case of the (K^-, π^+) reaction, only the total isospin $T = 3/2$ states can be populated. On the other hand, the (K^-, π^-) spectrum contains both $T = 3/2$ and $T = 1/2$ states. Here, the total spin in the four-body $\Sigma N N N$ system can be assumed to be $S = 0$ because the spin-flip amplitude is small in this reaction. Therefore, it can be interpreted that the ${}^4_{\Sigma}\text{He}$ bound state is originated by the attraction of $\Sigma N N N(T = 1/2, S = 0)$ channel.

In Ref. [23], the four body $\Sigma N N N$ potential is constructed based on the two body ΣN potentials. The isospin-spin averaged ΣN potential, $\bar{V}_{\Sigma N}$, in the four body $\Sigma N N N$ system can be decomposed as,

$$\Sigma N N N(T = 3/2, S = 0) : \bar{V}_{\Sigma N} = \frac{5}{18} V_{\frac{3}{2}0} + \frac{1}{2} V_{\frac{3}{2}1} + \frac{2}{9} V_{\frac{1}{2}0}, \quad (16)$$

$$\Sigma N N N(T = 1/2, S = 0) : \bar{V}_{\Sigma N} = \frac{4}{9} V_{\frac{3}{2}0} + \frac{1}{18} V_{\frac{1}{2}0} + \frac{1}{2} V_{\frac{1}{2}1}, \quad (17)$$

where V_{TS} denotes the two body ΣN potentials with the total isospin T and spin S in the two body ΣN system. By considering the difference between (K^-, π^-) and (K^-, π^+) spectra, the

$\Sigma NNN(T = 1/2, S = 0)$ channel would be attractive and the dominant components of this channel are $V_{\frac{3}{2}0}$ and $V_{\frac{1}{2}1}$. Therefore, it is also interpreted that $V_{\frac{3}{2}0}$ and $V_{\frac{1}{2}1}$ are the attractive potential. On the other hand, the heavier Σ -hypernucleus data exhibits no bound state peaks. It suggests that the isospin-spin averaged Σ -nucleus potential in the heavier system is repulsive. Therefore, $V_{\frac{3}{2}1}$ and $V_{\frac{1}{2}0}$ would be repulsive if the other $V_{\frac{3}{2}0}$ and $V_{\frac{1}{2}1}$ potentials are attractive. The conjecture regarding the isospin-spin dependence is consistent with the potentials constructed by Harada *et al* [23], quark-cluster model [25], and Lattice QCD [26]. Currently, it is anticipated to quantitatively extract the ΣN interaction strength for each isospin-spin channel separately.